pubs.acs.org/ac

analytical chemistry

December 15, 2015 Volume 87 Number 24

Acoustofluidic Fluorescence Activated Cell Sorter

ACS Publications
Most Trusted. Most Cited. Most Read.

www.acs.org

analytical chemistry

Article

pubs.acs.org/ac

Acoustofluidic Fluorescence Activated Cell Sorter

Ahmad Ahsan Nawaz,[†,‡] Yuchao Chen,[†] Nitesh Nama,[†] Ruth Helmus Nissly,[§] Liqiang Ren,[†] Adem Ozcelik,[†] Lin Wang,[∥] J. Philip McCoy,[⊥] Stewart J. Levine,[⊥] and Tony Jun Huang*[,†]

[†]Department of Engineering Science and Mechanics, The Pennsylvania State University, University Park, Pennsylvania 16802, United States

[‡]School of Mechanical and Manufacturing Engineering (SMME), National University of Sciences and Technology (NUST), Islamabad H-12, Pakistan

[§]Microscopy and Cytometry Facility, The Huck Institutes of the Life Sciences, The Pennsylvania State University, University Park, Pennsylvania 16802, United States

[∥]Ascent Bio-Nano Technologies Inc., State College, Pennsylvania 16801, United States

[⊥]National Heart, Lung, and Blood Institute (NHLBI), NIH, Bethesda, Maryland, United States

Supporting Information

ABSTRACT: Selective isolation of cell subpopulations with defined biological characteristics is crucial for many biological studies and clinical applications. In this work, we present the development of an acoustofluidic fluorescence activated cell sorting (FACS) device that simultaneously performs on-demand, high-throughput, high-resolution cell detection and sorting, integrated onto a single chip. Our acoustofluidic FACS device uses the "microfluidic drifting" technique to precisely focus cells/particles three dimensionally and achieves a flow of single-file particles/cells as they pass through a laser interrogation region. We then utilize short bursts (150 μs) of standing surface acoustic waves (SSAW) triggered by an electronic feedback system to sort fluorescently labeled particles/cells with desired biological properties. We have demonstrated continuous isolation of fluorescently labeled HeLa cells from unlabeled cells at a throughput of ~1200 events/s with a purity reaching 92.3 ± 3.39%. Furthermore, 99.18% postsort cell viability indicates that our acoustofluidic sorting technique maintains a high integrity of cells. Therefore, our integrated acoustofluidic FACS device is demonstrated to achieve two-way cell sorting with high purity, biocompatibility, and biosafety. We believe that our device has significant potential for use as a low-cost, high-performance, portable, and user-friendly FACS instrument.

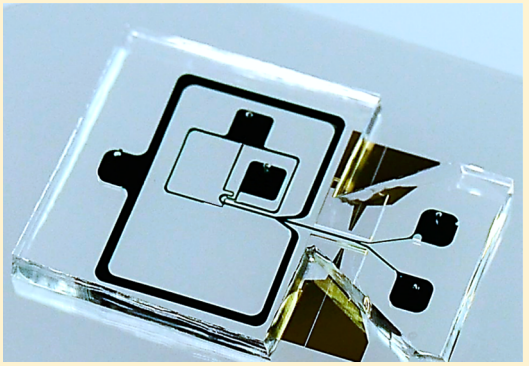

The ability to perform high-quality cell sorting is important in numerous fields, such as molecular biology, pathology, immunology, plant biology, stem cell biology, medical diagnostics, and drug screening.[1,2] In the last two decades, commercially available fluorescence activated cell sorting (FACS) instruments have emerged as a powerful tool for detection and isolation of desired cell populations with high purity and high throughput.[3,4] The commercial FACS instruments, although fast and reliable, rely on a high-pressure coaxial sheath flow for focusing and droplet formation for sorting of cells, which could negatively impact cell viability.[4−6] Moreover, conventional droplet-based FACS can often result in biohazardous aerosol formation, which can render the operator at risk of infection and contamination. Recently, the International Society for Advancement of Cytometry (ISAC) highlighted the need to follow stringent biosafety guidelines for FACS instrument operation due to aerosol formation of possibly contaminated or infectious samples.[7] Furthermore, high cost of equipment, bulky size, and the requirement of trained personnel for operation also limit commercial FACS instruments' use to large centralized laboratories, thereby inhibiting their accessibility in resource-poor settings.[8−13] These concerns have led to a significant research effort toward miniature closed-loop sorting approaches which completely omit cell encapsulation within droplets and aerosol formation.[14,15]

Microfluidics promises to overcome these drawbacks by offering inexpensive, mass-producible, disposable chips that utilize closed-loop, aerosol-free, on-chip sorting approaches.[16−21] Additionally, microfluidic approaches allow handling of small numbers of cells[22] and reduced reagent consumption,[23−25] as well as the possibility to combine sorting with other on-chip functionalities such as polymerase chain reaction (PCR),[26−29] sample preparation,[30] and/or cell incubation.[31]

Several microfluidic sorting mechanisms have been employed to achieve on-chip sorting.[32−37] Fu et al. demonstrated electroosmotic microfluidic FACS which achieved enrichment of

Received: June 26, 2015
Accepted: August 21, 2015
Published: September 2, 2015

DOI: 10.1021/acs.analchem.5b02398
Anal. Chem. 2015, 87, 12051−12058

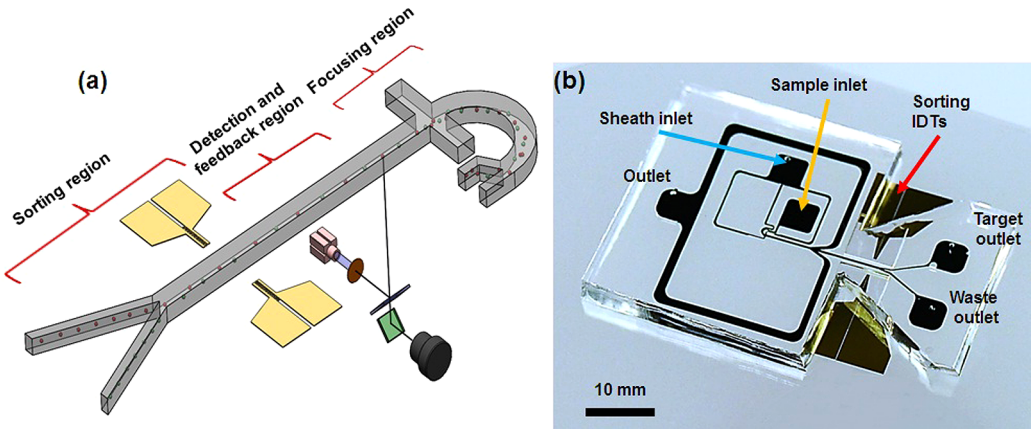

Figure 1. (a) Schematic of the acoustofluidic FACS device (bifurcation channel is not shown for simplicity). The detection region includes a 488 nm solid-state laser integrated within an optical microscope. A PMT is attached to the microscope C-mount. The detection system provides feedback to the sorting IDTs which generate a trigger signal to sort the particles/cells to the desired outlet. (b) Small footprint of the device. The device includes a single inlet for the sheath fluid, a single inlet for sample fluid, and a pair of IDTs for sorting the particles/cells.

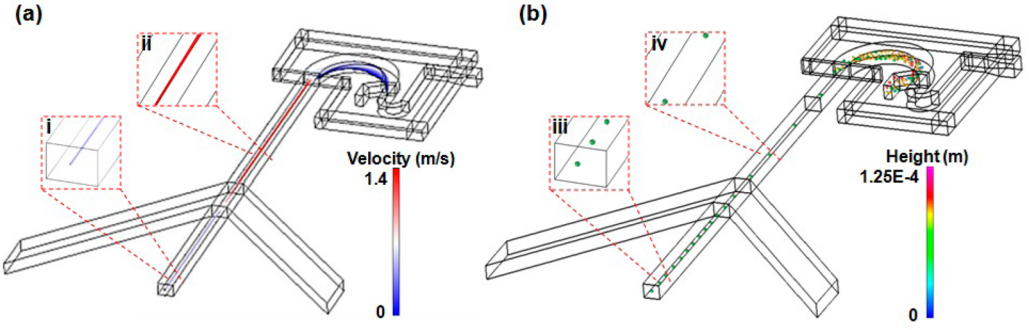

Figure 2. (a) Simulation of 5 μM fluorescein solution injected into the sheath fluid stream in the device. The isocurve profile indicates that effective 3D focusing of the sample fluid is achieved and the midstream velocity decreases after the bifurcated outlets. Insets i and ii show a magnified image of the channel before and after the bifurcation, respectively. (b) Simulation of 10 μm polystyrene beads focusing into a single-file line of particles as they approach the channel downstream. Insets iii and iv show a magnified view of particles flowing in the channel before and after bifurcation, respectively. All downstream particles are green-colored indicating their channel middle position with respect to channel height. Moreover, the particle interspacing distance decreases as the particles flow pass the bifurcation region, which also signifies that the midstream velocity decreases.

particles and bacteria up to 96-fold at a throughput of 20 events/s.[38] In another study, the same group used hydrodynamic pressure to achieve similar enrichment at a sorting throughput of 40 events/s.[39] Fiedler et al. used a miniaturized array of electrodes to demonstrate that alternating current (AC) fields generate forces that can be utilized for separation of particles.[40] Wang et al. demonstrated that optical forces could be utilized as switches to route cells into desired outlets in a microfluidic channel.[41] These recent developments have shown that microfluidic FACS can provide high-purity enrichment of target cells/particles while also omitting the aerosol formation.

Since low-power acoustic waves allow precise cell manipulation while preserving the integrity and functions of living cells, several groups have utilized acoustic approaches to achieve higher throughput while maintaining high purity.[42−44] Johansson et al. demonstrated that differences in fluid densities can be exploited for sorting cells via acoustic radiation force.[45] Recently, Schmid et al. used two-dimensional (2D) hydrodynamic focusing to focus pico-liter droplets followed by sorting that utilizes 330 μs bursts of traveling surface acoustic waves (TSAW) to demonstrate a throughput of 3000 droplets/s without any sorting errors.[46] However, in this approach, high-throughput sorting of mouse melanoma cells without droplet encapsulation was limited by clustering of cells.

In this work, we demonstrate an acoustofluidic FACS device (Figure 1) that integrates "microfluidic drifting"-based three-dimensional (3D) prefocusing of cells/particles and short bursts of standing surface acoustic waves (SSAW)[47−52] onto a single chip to achieve on-demand, high-throughput, high-purity sorting. We have previously demonstrated a 3D submicrometer precision focusing via a "microfluidic drifting" phenomenon which also provided high-throughput immunological analysis.[53−57] In this work, we build upon our previous work by combining the "microfluidic drifting" focusing approach with a SSAW-based sorting technique. We modified the device to achieve a slower midstream velocity to allow for SSAW to act on cells/particles for longer times and effectively direct them into a target channel (Figure 2). Utilizing interdigital transducers (IDTs) with short active regions (120 μm) allowed short bursts (150 μs) of SSAW. With this setup, a sorting purity of up to 92.3 ± 3.39% for HeLa cell lines at a total throughput of ∼1200 events/s was demonstrated. Moreover, 99.18% postsort cell viability indicated that our acoustofluidic cell sorter can maintain the cell integrity during the cell sorting process. The acoustofluidic FACS device presented in this work offers the simultaneous abilities of high-resolution cytometric detection and high-purity, high-throughput cell sorting.

DOI: 10.1021/acs.analchem.5b02398
Anal. Chem. 2015, 87, 12051−12058

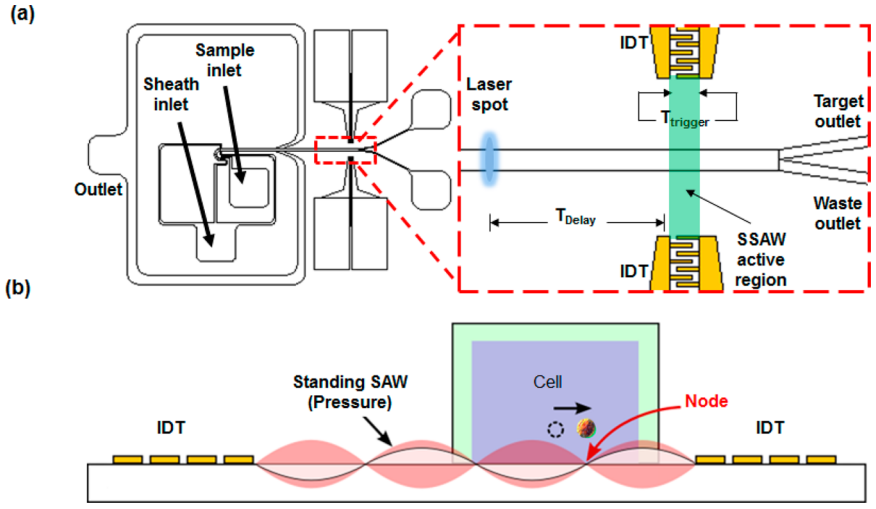

Figure 3. (a) Schematic of the acoustofluidic FACS device indicating the focusing region. The expanded image indicates the laser spot, IDT region, and sorting outlets. (b) Channel cross-section illustrating the SSAW sorting mechanism. Constructive interference of surface acoustic waves originating from both IDTs results in SSAW. Upon SSAW activation, cells/particles focused at channel middle position tend to move toward the pressure node, leading them into the target outlet.

MATERIALS AND METHODS

Device Design and Modeling. Figure 1a shows the schematic of the acoustofluidic FACS device indicating different regions, i.e., focusing region, detection region, and sorting region. Figure 1b indicates small footprint of the device. In this work, we utilized a modified "microfluidic drifting"-based flow cytometry device for focusing the cells/particles three dimensionally. Specifically, the design modification aimed at reducing the velocity of cells/particles as they crossed the SSAW active region to allow them to experience SSAW generated acoustic radiation force for longer duration. The operational parameters are chosen to allow the cells/particles to flow through the SSAW active region for a specific amount of time causing the displacement of the cell into the target outlet.

Previously, we demonstrated a single sheath fluid inlet device for high-precision 3D focusing of cells/particles, where particle midstream velocity reached 1.4 m/s.[55] To achieve synchronization between the detection and sorting of particles/cells, it was essential to reduce midstream velocity while maintaining 3D focusing of cells/particles. We utilized CFD-ACE+ software (ESI Group) to design a downstream-bifurcated channel such that the flow velocity of the sample fluid (midstream) was reduced, as shown in Figure 2. We ensured convergence of our simulation results by employing a relative convergence criterion of 10^{-6} for the simulations. In the simulations, 5 μM fluorescein was used as sample fluid and deionized water was used as sheath fluid. Figure 2a illustrates that the channel midstream velocity reduced to 0.8 m/s in the postbifurcation region. Insets i and ii in Figure 2a show magnified images of the sample stream velocity before (1.4 m/s) and after (0.8 m/s) the bifurcation, respectively. In our devices, the bifurcation channels were recombined to form a single outlet to maintain equal backpressure of the fluid to ensure particle focusing within the channel. Figure 2b illustrates the simulation results elucidating that the particles maintain their focused position once they cross the bifurcation region. This is indicated by the green color of the particles representing the channel middle position. Insets iii and iv in Figure 2b depict magnified images of polystyrene beads before and after bifurcation, respectively. The reduced interparticle distance after the bifurcation also signifies the reduced velocity.

Device Fabrication. The device was fabricated through standard soft-lithography and mold-replica techniques.[58] Silicon wafer was spun-coated with SU8 photoresist (~128 μm in thickness) to develop the master mold. Hydrophobic coating of $1H,1H,2H,2H$-perfluorooctyl-trichlorosolane vapor (Sigma-Aldrich) was conducted to facilitate peel-off of the polydimethylsiloxane (PDMS) layer. After pouring PDMS on the mold, degassing was done to remove all air bubbles. Oven curing of PDMS at 65 °C was conducted to fabricate the microfluidic channels. The IDTs were fabricated on a 128° Y-cut lithium niobate ($LiNbO_3$) substrate via a standard photolithography process followed by depositing two thin-layer metals (Cr/Au, 5 nm/50 nm) by e-beam evaporation (RC0021, Semicore, USA). Each interdigital transducer (IDT) had 50 pairs of electrodes, effective width of 120 μm, and an excitation frequency of 33.28 MHz. The acoustic power and frequency (−2.8 dBm and 33.8 MHz, respectively) of SSAW were kept constant. Higher acoustic power resulted in bubble generation within the microfluidic channel which disrupted the cell/particle sorting. During the metal deposition process, several markers for alignment of the PDMS channel were also deposited on the substrate so that the pressure node was positioned in alignment with the target outlet. After plasma treatment, the PDMS channel fabricated by soft lithography was bonded to the substrate. After removing the PDMS layer from the mold, a 0.7 mm Harris Uni-Core (Ted Pella Inc. USA) was used to punch circular inlets and outlets. The inlets were connected via polyethylene tubes to syringe pumps (KD Scientific, USA) to supply sheath fluid and sample to the device. The free ends of tubing from the target outlet and waste were placed in two separate collection vials.

Optical Detection Setup and Sorting Feedback System. The experiments were conducted using a homemade laser-induced fluorescence (LIF) system such that an inverted microscope (TE2000-U, Nikon, Japan) was fitted with a photomultiplier tube (PMT, H6780-20, Hamamatsu, Japan) to the C-mount. A schematic of the optical setup[59−61] and the device is shown in Figure 1a,b. A laser light (10 mW at 488 nm,

DOI: 10.1021/acs.analchem.5b02398
Anal. Chem. 2015, 87, 12051−12058

Bluesky Research, USA) was introduced via fluorescence lamp house into the microscope. A 20× objective lens focused the laser beam into a spot of approximately 40 μm diameter. The emission signal (from fluorescent beads or fluorescently labeled cells) was transmitted via the same optical path through the dichroic mirror onto the PMT, which was fitted with a 525 nm ±10 nm bandpass filter to allow only these wavelengths of fluorescent light onto the PMT for measurement. The signals collected by the PMT were delivered to a flow cytometry data acquisition system (Azurite, DarklingX, USA), which provided real-time data acquisition. The PMT detected fluorescent signal height in terms of voltages, which were converted into intensity. In a count vs fluorescence intensity histogram generated by the data acquisition system, a gate was drawn along the x-axis as shown in Figure S2. Cells/particles with fluorescence values within the gated region resulted in 3.3 V trigger signal generation that was fed into the trigger input connection port of a function generator (AFG3102C, Tektronix, USA). On-demand sorting can be observed with this setup, allowing any chosen object to be selected for sorting. Preset resonance frequency (33.8 MHz) and amplitude (−2.8 dBm) of the output signal was directed into the amplifier which in turn was connected to the pair of IDTs on the lithium niobate substrate.

In our setup, the laser spot was kept approximately 800 μm away from the SSAW active sorting region. The SSAW active region spanned 120 μm in length, while the outlets (target and waste) were approximately 200 μm away from the SSAW active region (schematic in Figure 3; not to scale). On the basis of the particle velocity of 0.8 m/s and the distance between the laser spot and the SSAW active region (800 μm), T_{delay} and $T_{trigger}$ were set to 1 and 0.15 ms, respectively.

Flow Cytometry Data Acquisition and Analysis. The analysis of presort and postsort samples was conducted with a commercial flow cytometer (FC500, Beckman Coulter, USA). The flow cytometer uses a 488 nm laser emission. Forward scatter (FSC), side scatter (SSC), and fluorescent emission (FL) signals were collected for analysis. The data collected by the flow cytometer was analyzed by FlowJo software (FlowJo, LLC, Oregon, USA). For calculating the purity of the target and waste outlets, a gate was constructed around the unstained population of the control unstained sample results. The same gate function was then transferred to stained sample result files. The purity of the sample is defined as[62]

$$\text{purity} = \frac{\text{number of fluorescent cells or particles in target outlet}}{\text{total number of cells or particles analyzed}} \quad (1)$$

while the recovery is defined as[62]

$$\text{recovery}\,\% = 100 - \frac{\text{purity of waste outlet}\,(\%)}{\text{initial purity}\,(\%)} \quad (2)$$

SSAW Sorting Mechanism. SSAW are sound waves produced on the surface of a lithium niobate substrate when excited by a pair of IDTs deposited onto a piezoelectric substrate. Figure 3a illustrates the top-view of the device design indicating the position of IDTs. The expanded (red dotted rectangular) region delineates the enlarged view of IDTs while also showing the times "T_{delay}" and "$T_{trigger}$". "T_{delay}" signifies the time the particle takes to travel from the detection point to the SSAW active region, while "$T_{trigger}$" is particle flight time through the SSAW active region. Both "T_{delay}" and "$T_{trigger}$" are set based on the particle velocity. The two counter-propagating SAWs originating from each IDT interfere constructively to generate a SSAW on the substrate as shown in the schematic in Figure 3b. Upon encountering the liquid flowing in the PDMS channel, these acoustic waves leak into the liquid such that pressure nodes and antinodes are formed within the channel.

The primary acoustic radiation force acting upon the particles suspended in fluid is given by[63]

$$F_r = -\left(\frac{\pi p_0^{\,2} V_c \beta_w}{2\lambda}\right)\phi(\beta, \rho)\sin(2kx) \quad (3)$$

$$\phi(\beta, \rho) = \frac{5\rho_c - 2\rho_w}{2\rho_c + \rho_w} - \frac{\beta_c}{\beta_w} \quad (4)$$

where p_0, λ, V_c, β_c, β_w, ρ_c, and ρ_w are the acoustic pressure, wavelength, volume of the particle, compressibility of the particle, compressibility of the fluid, density of the particle, and density of the fluid, respectively, and ϕ is the acoustic contrast factor that defines whether the particle will translate to pressure node ($\phi > 0$) or pressure antinode ($\phi < 0$).

The target and waste outlets were designed such that their junction was offset by 10 μm (the width of the waste outlet was larger than that of the target outlet), thereby leading the focused file of cells/particles into the waste outlet when the SSAWs are in the "OFF" state. The PDMS channel was positioned on the substrate such that the actuation of SSAW and subsequent displacement of particles toward the pressure node position leads the cells/particles into the target outlet.

Sample Preparation. Flow-Check (10 μm, diameter) Fluorospheres (Beckman Coulter, Inc. USA) were used for characterization of fluorescent signals and calibration of the device. For sorting beads, a 1:1 (v/v) of 7.32 μm Dragon Green fluorescent polystyrene beads were mixed with nonfluorescent beads (Bangs Laboratories, USA) and diluted in 0.01% sodium dodecyl sulfate (SDS) solution such that the final concentration was 4.70×10^6 beads/mL. For sorting HeLa cells (ATCC), 1 mL of calcein AM (0.5 mmol/L, Life Technologies, USA) was added to 1 mL of cells suspended in phosphate buffer saline (PBS), followed by incubation at room temperature for 30 min. Stained cells were then centrifuged and resuspended in 1 mL of PBS. Unlabeled HeLa cells were also washed in PBS and mixed with stained HeLa cells. From this cell sample, 400 μL of the mixed cell solution was used for commercial flow cytometric analysis which indicated 51.2% stained HeLa cells. Before sorting via our acoustofluidic FACS device, the mixture of labeled and unlabeled HeLa cells was analyzed via a hemocytometer indicating total concentration of 3.76×10^6 cells/mL.

To test postsorting viability, HeLa cells were collected from the target outlet with SSAW continuously "ON". The collected cells were incubated with 1 μL of propidium iodide (PI) (concentration of 1 μg/mL) for 30 min at room temperature. For the viability positive control, ethanol (70% by volume) was added to unsorted HeLa cells suspended in PBS followed by staining with 1 μL of PI solution.

RESULTS AND DISCUSSION

Particle Focusing. Coefficient of variation (the ratio of standard deviation to mean) is an indicator of particle-focusing precision. Low CV, indicating tight focusing of particles/cells, is essential for high-resolution data analysis and synchronization between detection and the sorting action. Another important factor is a small distance between the laser spot and the SSAW active region, which ensures that a single particle/cell passes

DOI: 10.1021/acs.analchem.5b02398
Anal. Chem. 2015, 87, 12051−12058

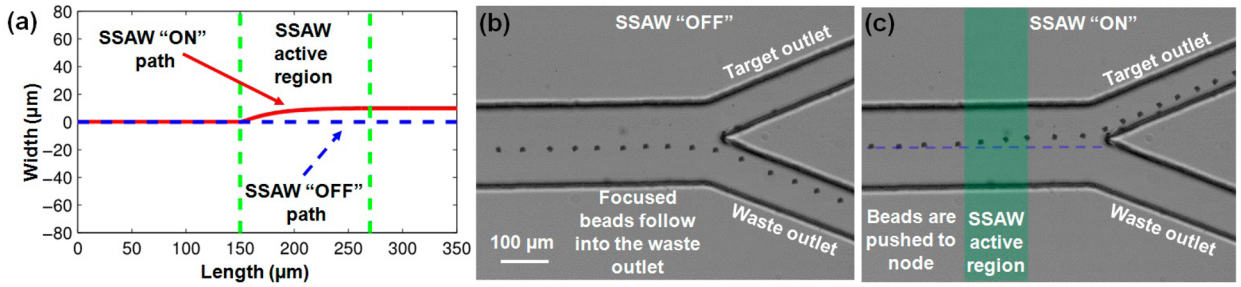

Figure 4. (a) Simulation results indicating the trajectory of particles. Particles prefocused in the channel middle position deflect ~15 μm upon entering the SSAW active region in the SSAW "ON" state. (b) z-stacked image indicating particle trajectory when SSAW is in the "OFF" state leading the particle into the waste outlet. (c) z-stacked image showing trace of particle trajectory when SSAW is in the "ON" state. The polystyrene bead is pushed toward the node position and then leads into the target outlet. For comparison, the dashed blue line shows the particle trajectory when SSAW was "OFF".

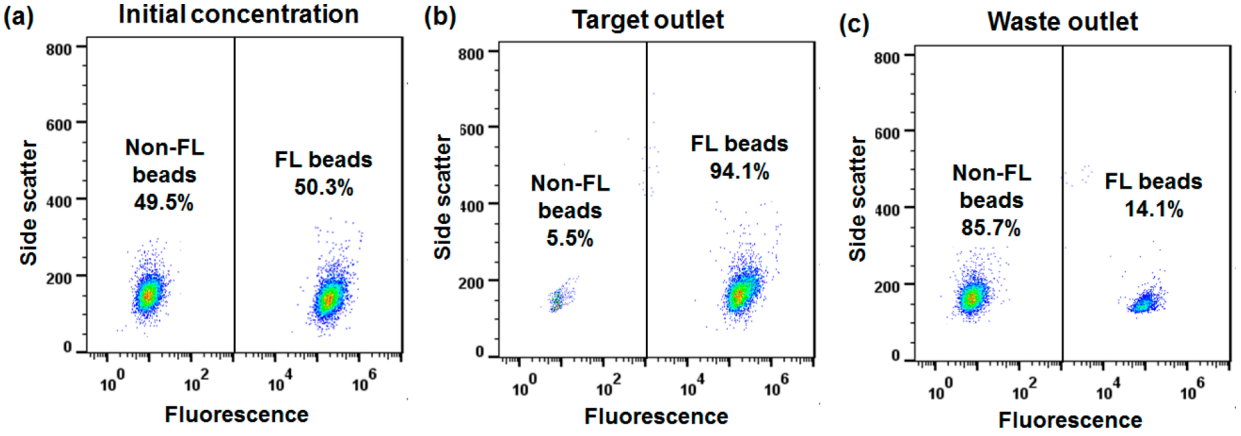

Figure 5. (a) Initial concentration of a mixture of fluorescent and nonfluorescent polystyrene beads analyzed via commercial flow cytometry was 50.3% and 49.5%, respectively. (b) Postsort commercial flow cytometric analysis of the target outlet indicated a purity of 94.1% fluorescent while 5.5% are nonfluorescent polystyrene beads. (c) Analysis of waste outlet indicated that 14.1% fluorescent polystyrene beads were not sorted.

through the SSAW active region during the SSAW activation period. The performance of the acoustofluidic FACS device was first characterized by using Flow-Check Fluorospheres. In the FACS device setup, the laser spot was focused onto the z-plane where the beads were located by adjusting the laser focal point until the minimum possible CV for fluorescent signal was achieved. To compare the precision of the particle focusing at various locations throughout the device, the laser spot was set at different positions of the microfluidic channel. When the laser spot was positioned before the bifurcation (position 1, Figure S1a), the fluorescence signal CV was measured to be 2.21% (Figure S1b). Moving the microscope stage to position the laser spot in the postbifurcation region (position 2, Figure S2a) ~800 μm before the IDT active region indicated a CV of 2.44% (Figure S1c). This result demonstrated that tight particle focusing was maintained after velocity reduction caused by the bifurcation. Thus, 3D focusing of the particles was preserved as they flow toward the SSAW active region, which could minimize multiple particles coincidently entering the SSAW active region.

Simulation Results vs Experimental Results. Figure 4a–c shows the comparison between simulation and experimental results of 10 μm polystyrene bead deviation from the focused midstream position upon SSAW activation. The simulation results in Figure 4a indicate approximately 15 μm lateral deviation in the path of polystyrene bead from midstream (indicated by red line) upon SSAW activation. Figure 4b is a z-stack image of time lapse images indicating the path followed by a polystyrene bead when SSAW is "OFF". Figure 4c shows a z-stacked image of time lapse images elucidating polystyrene bead trajectory at the instance when SSAW is in the "ON" state. The video S3 shows that polystyrene beads flow into the waste outlet when SSAW is inactive while they are led into the target outlet when the SSAW is actuated.

From Figure 4b, it is seen that polystyrene beads start to deviate before the SSAW active region, due to divergence of the SSAW from the IDTs. An experimentally observed SSAW-influence region of ~220 μm, combined with the particle velocity of 0.8 m/s, leads to $T_{trigger}$ = 312 μs that limits the maximum throughput to 3200 events/s. Under these conditions, SSAW influences a 1.5 pL volume of fluid. This leads to a maximum particle concentration of 6.7 × 10^8/mL that can be sorted before the coincidences will limit the sorting performance. Reducing the SSAW active region span could further improve sorting throughput by allowing less separation between two consecutive particles, albeit that might necessitate the use of increased power to achieve sufficient deflection for sorting especially for smaller sized cells/particles (eq 3). By optimizing the design and wavelength of the IDTs and the particle velocity, shorter $T_{trigger}$ could be realized leading to higher throughputs.

Particle/Cell Sorting. Next, sorting fluorescent from nonfluorescent polystyrene beads was demonstrated. A mixture of fluorescent and nonfluorescent polystyrene beads was

DOI: 10.1021/acs.analchem.5b02398
Anal. Chem. 2015, 87, 12051−12058

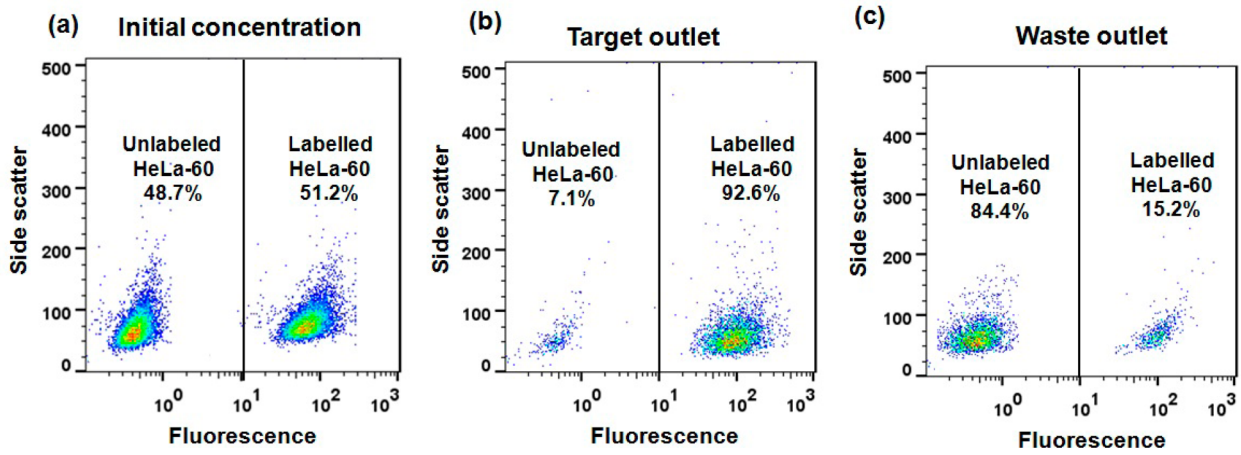

Figure 6. (a) Initial concentration of fluorescently labeled and unlabeled HeLa cells was determined via commercial flow cytometry as 51.2% and 48.7%, respectively. (b) Postsort commercial flow cytometric analysis of the target outlet indicated a purity of 92.6% labeled and 7.1% unlabeled cells, respectively. (c) Waste outlet analysis indicated 84.4% unlabeled and 15.2% labeled HeLa cells.

analyzed via a commercial flow cytometer indicating 50.3% and 49.5% concentration of former and later, respectively, shown in Figure 5a. The same concentration mixture was then injected at a flow rate of 20 μL/min from the sample inlet into the acoustofluidic FACS device. A throughput of ∼1500 particles/s was achieved during the sorting while samples were simultaneously collected from target and waste outlets. This was followed by commercial flow cytometric analysis for evaluation of the sorting performance. Target outlet collected sample analysis indicated 94.1 ± 2.4% purity of fluorescent polystyrene bead particles (Figure 5b). Waste outlet contained 85.7% nonfluorescent and 14.3% fluorescent beads, as shown in Figure 5c. Eq 2 was used to calculate 98.27% recovery. These results indicate that our acoustofluidic FACS device can achieve high-throughput sorting of polystyrene beads while maintaining a high level sort purity.

The performance of the SSAW-based sorter was also tested by sorting calcein-AM stained HeLa cells from unlabeled HeLa cells. An initial concentration of 51.2% and 48.7% of labeled and unlabeled HeLa cells, respectively, was determined by analyzing the cell mixture via a commercial flow cytometer, as indicated in Figure 6a. The same concentration cell mixture was then injected at a flow rate of 20 μL/min for sorting via our acoustofluidic FACS device. At a throughput of ∼1200 cells/s, sort was collected from target and waste outlet followed by their commercial flow cytometry for performance evaluation of our acoustofluidic FACS device. The target outlet showed a purity reaching ∼92.3 ± 3.39% indicated in Figure 6b. Analysis of the waste outlet demonstrated 80.4% unlabeled HeLa cells and 19.6% labeled HeLa cells (Figure 6c). From Eq 2, a 98.43% recovery was calculated. This result further confirms that both high throughput and high purity are attainable with our acoustofluidic sorting approach.

Viability Test of SSAW Exposed Cells. Viability of the cells is pivotal when sorting cells of interest. Viability studies are done for the determination of living cells and those which are dead or have damaged cell membrane. Commercial FACS may damage cells, especially fragile cells, due to factors such as large shear stress from hydrodynamic forces and high voltages used for deflecting the droplet-encapsulated cells.[6] To perform a viability analysis, unstained HeLa cells were passed through our acoustofluidic FACS device while SSAW was permanently in the "ON" state such that all the cells were deflected into the target outlet. The HeLa cells were collected at the target outlet and stained with PI, which can only bind to cells if the cell membrane is damaged. No staining was expressed by 99.18% (2.96% − 2.14% = 0.82%; 100% − 0.82% = 99.18% survival) of the HeLa cells as shown in the histogram plot in Figure 7

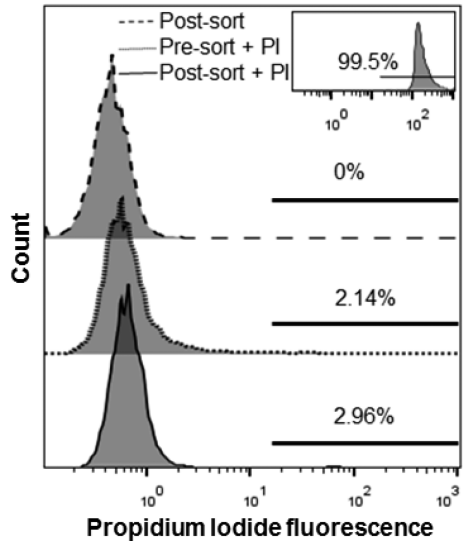

Figure 7. HeLa cell viability results after subjection to SSAW from the acoustofluidic FACS device. Postsort HeLa cells with PI staining is represented with continuous line histogram. Postsort, presort with PI, and ethanol treated with PI staining controls are represented by dashed, dotted, and inset histograms, respectively. 99.18% (2.96% − 2.14% = 0.82%; 100% − 0.82% = 99.18% survival) postsort HeLa cell viability as they undergo acoustic force exposure through the device.

(postsort + PI; continuous line histogram). The control experiments included positive control (ethanol treated dead cells; inset in Figure 7), presorted cells with PI addition (dotted line histogram), and postsorted cells without PI addition (dashed line histogram). The results indicate that, for the power intensity (−2.8 dBm) and the frequency (33.8 MHz) employed in our acoustofluidic FACS, the viability of the cells remains intact.

DOI: 10.1021/acs.analchem.5b02398
Anal. Chem. 2015, 87, 12051−12058

CONCLUSION

In this work, we demonstrated an on-demand, high-purity, high-throughput, aerosol-free acoustofluidic FACS device. We utilized a modified design of our "microfluidic drifting" approach to achieve 3D prefocusing of cells/particles prior to sorting. CV measurement of the fluorescent polystyrene beads flowing through the microfluidic device was found to be 2.44%. A sorting purity reaching ~92.3 ± 3.39% at a total throughput of 1200 cells/s for fluorescently labeled HeLa cells was demonstrated. 99.18% of the cells that passed through our acoustofluidic device and experienced acoustic radiation force remained viable. 3D prefocusing of cells/particles, short SSAW bursts, and smaller distances between laser spot, SSAW active region, and outlets were crucial in increasing the probability of one cell/particle at a time flowing into the SSAW active region. These factors led to higher purity sorting without compromising high throughput. We believe that optimizing the device design could further improve purity and throughput. Future work will aim at optimization including IDT design, wavelength, using channel material with higher SSAW transmittance, and shrinking the distances between the laser spot, SSAW active region, and outlets. Furthermore, channel and IDT designs that allow three, four, or five-way sorting could also be envisioned with our acoustofluidic sorting approach. Hence, besides being aerosol-free and biologically friendly to sorted cells, our acoustofluidic FACS device possesses the potential to serve as a miniature, high-throughput, high-purity cell sorter.

ASSOCIATED CONTENT

Supporting Information

The Supporting Information is available free of charge on the ACS Publications website at DOI: 10.1021/acs.analchem.5b02398.

Results on pre- and postbifurcation without calibration; azurite sort gating (PDF)

Polystyrene beads flowing through the acoustofluidic FACS device (AVI)

AUTHOR INFORMATION

Corresponding Author

*Fax: 814-865-9974. Tel: 814-863-4209. E-mail: junhuang@psu.edu.

Notes

The authors declare no competing financial interest.

ACKNOWLEDGMENTS

We thank Dr. Peng Li for helpful discussions and Mark Naivar for his guidance on the Azurite data acquisition system. This research was supported by National Institutes of Health (1 R01 GM112048-01A1 and 1R33EB019785-01), National Science Foundation (IIP-1534645), and the Penn State Center for Nanoscale Science (MRSEC) under Grant DMR-1420620. J.P.M. and S.J.L. are supported by the NHLBI Division of Intramural Research. Components of this work were conducted at the Penn State node of the NSF-funded National Nanotechnology Infrastructure Network (NNIN) and Microscopy and Cytometry Facility.

REFERENCES

(1) Davey, H. M.; Kell, D. B. *Microbiol. Rev.* **1996**, *60* (4), 641−696.
(2) Eisenstein, M. *Nature* **2006**, *441* (7097), 1179−1185.
(3) BD Influx Cell Sorter; www.bdbiosciences.com.
(4) Takahashi, K.; Hattori, A.; Suzuki, I.; Ichiki, T.; Yasuda, K. *J. Nanobiotechnol.* **2004**, *2* (1), 5.
(5) Milner, A. E.; Vaughan, A. T.; Clark, I. P. *Radiat. Res.* **1987**, *110* (1), 108−117.
(6) Leary, J. F. In *Current Protocols in Cytometry*; Robinson, J. P., Darzynkiewicz, Z., Dobrucki, J., Hyun, W. C., Nolan, J. P., Orfao, A., Rabinovitch, P. S., Eds.; John Wiley & Sons, Inc.: Hoboken, NJ, USA, 2001.
(7) Holmes, K. L.; Fontes, B.; Hogarth, P.; Konz, R.; Monard, S.; Pletcher, C. H.; Wadley, R. B.; Schmid, I.; Perfetto, S. P. *Cytometry, Part A* **2014**, *85* (5), 434−453.
(8) Tüdös, A. J.; Besselink, G. J.; Schasfoort, R. B. *Lab Chip* **2001**, *1* (2), 83−95.
(9) Wang, S.; Inci, F.; De Libero, G.; Singhal, A.; Demirci, U. *Biotechnol. Adv.* **2013**, *31* (4), 438−449.
(10) Shapiro, H. M. *Practical Flow Cytometry*; John Wiley & Sons, Inc.: Hoboken, NJ, USA, 2003.
(11) Morris, K. *Lancet Infect. Dis.* **2009**, *9* (5), 274.
(12) Pop-Eleches, C.; Thirumurthy, H.; Habyarimana, J. P.; Zivin, J. G.; Goldstein, M. P.; de Walque, D.; MacKeen, L.; Haberer, J.; Kimaiyo, S.; Sidle, J.; Ngare, D.; Bangsberg, D. R. *AIDS* **2011**, *25* (6), 825−834.
(13) Maleki, T.; Fricke, T.; Quesenberry, J.; Todd, P.; Leary, J. F. In *Proceedings of SPIE*; Becker, H., Gray, B. L., Eds.; SPIE: Bellingham WA, 2012; p 82510C.
(14) Schmid, I.; Hultin, L. E.; Ferbas, J. *Curr. Protoc. Cytom.* **2001**, DOI: 10.1002/0471142956.cy0303s01.
(15) Gray, D. W. R.; Gohde, W.; Carter, N.; Heiden, T.; Morris, P. J. *Diabetes* **1989**, *38* (Supplement1), 133−135.
(16) Godin, J.; Chen, C.-H.; Cho, S. H.; Qiao, W.; Tsai, F.; Lo, Y.-H. *J. Biophotonics* **2008**, *1* (5), 355−376.
(17) Ozcelik, A.; Ahmed, D.; Xie, Y.; Nama, N.; Qu, Z.; Nawaz, A. A.; Huang, T. J. *Anal. Chem.* **2014**, *86* (10), 5083−5088.
(18) Reece, L. M.; Sanders, L.; Kennedy, D.; Guernsey, B.; Todd, P.; Leary, J. F. *Proc. SPIE* **2010**, *7568*, 75680P-1−75680P-12.
(19) Geheb, B. R.; Grafton, M. M. G.; Jang, J.; Reece, L. M.; Leary, J. F.; Kwon, J. K.; Jung, B. In *IEEE/NIH Life Science Systems and Applications Workshop, LiSSA 2009*, April 9−10, 2009; pp 40−43.
(20) Grafton, M. M.; Geheb, B.; Jang, J. H.; Chuang, H.-S.; Rajdev, P.; Reece, L. M.; Irazoqui, P. P.; Wereley, S. T.; Jung, B.; Leary, J. F. *Proc. SPIE* **2009**, *7207*, 72070A−72070A-9.
(21) Wu, T. H.; Chen, Y.; Park, S. Y.; Hong, J.; Teslaa, T.; Zhong, J. F.; Di Carlo, D.; Teitell, M. A.; Chiou, P. Y. In *Proceedings of the IEEE International Conference on Micro Electro Mechanical Systems (MEMS)*, Jan 29 to Feb 2, 2012; pp 1097−1100.
(22) Shapiro, H. M. *Practical Flow Cytometry*; Wiley-Liss: New York, 2003.
(23) Chen, Y.; Chung, A. J.; Wu, T. H.; Teitell, M. A.; Di Carlo, D.; Chiou, P. Y. *Small* **2014**, *10* (9), 1746−1751.
(24) Chen, Y.; Wu, T.-H.; Kung, Y.-C.; Teitell, M. a; Chiou, P.-Y. *Analyst* **2013**, *138* (24), 7308−7315.
(25) Wu, M.-H.; Huang, S.-B.; Lee, G.-B. *Lab Chip* **2010**, *10* (8), 939−956.
(26) Waters, L. C.; Jacobson, S. C.; Kroutchinina, N.; Khandurina, J.; Foote, R. S.; Ramsey, J. M. *Anal. Chem.* **1998**, *70* (1), 158−162.
(27) Kopp, M. U.; de Mello, A. J.; Manz, A. *Science* **1998**, *280* (5366), 1046−1048.
(28) Ma, S.; Loufakis, D. N.; Cao, Z.; Chang, Y.; Achenie, L. E. K.; Lu, C. *Lab Chip* **2014**, *14* (16), 2905−2909.
(29) Liao, C. S.; Lee, G. B.; Liu, H. S.; Hsieh, T. M.; Luo, C. H. *Nucleic Acids Res.* **2005**, *33* (18), No. e156.
(30) Li, P. C. H.; Harrison, D. J. *Anal. Chem.* **1997**, *69* (8), 1564−1568.
(31) Inoue, I.; Wakamoto, Y.; Moriguchi, H.; Okano, K.; Yasuda, K. *Lab Chip* **2001**, *1* (1), 50−55.
(32) Oakey, J.; Applegate, R. W.; Arellano, E.; Di Carlo, D.; Graves, S. W.; Toner, M. *Anal. Chem.* **2010**, *82* (9), 3862−3867.
(33) Skommer, J.; Akagi, J.; Takeda, K.; Fujimura, Y.; Khoshmanesh, K.; Wlodkowic, D. *Biosens. Bioelectron.* **2013**, *42*, 586−591.

DOI: 10.1021/acs.analchem.5b02398
Anal. Chem. 2015, 87, 12051−12058

(34) Ding, X.; Lin, S.-C. S.; Lapsley, M. I.; Li, S.; Guo, X.; Chan, C. Y.; Chiang, I.-K.; Wang, L.; McCoy, J. P.; Huang, T. J. *Lab Chip* **2012**, *12* (21), 4228−4231.
(35) Cao, Z.; Chen, F.; Bao, N.; He, H.; Xu, P.; Jana, S.; Jung, S.; Lian, H.-Z.; Lu, C. *Lab Chip* **2013**, *13*, 171.
(36) Applegate, R. W.; Marr, D. W. M.; Squier, J.; Graves, S. W. *Opt. Express* **2009**, *17* (19), 16731−16738.
(37) Yang, S.-Y.; Hsiung, S.-K.; Hung, Y.-C.; Chang, C.-M.; Liao, T.-L.; Lee, G.-B. *Meas. Sci. Technol.* **2006**, *17* (7), 2001−2009.
(38) Fu, A. Y.; Spence, C.; Scherer, A.; Arnold, F. H.; Quake, S. R. *Nat. Biotechnol.* **1999**, *17* (11), 1109−1111.
(39) Fu, A. Y.; Chou, H.-P.; Spence, C.; Arnold, F. H.; Quake, S. R. *Anal. Chem.* **2002**, *74* (11), 2451−2457.
(40) Fiedler, S.; Shirley, S. G.; Schnelle, T.; Fuhr, G. *Anal. Chem.* **1998**, *70* (9), 1909−1915.
(41) Wang, M. M.; Tu, E.; Raymond, D. E.; Yang, J. M.; Zhang, H.; Hagen, N.; Dees, B.; Mercer, E. M.; Forster, A. H.; Kariv, I.; Marchand, P. J.; Butler, W. F. *Nat. Biotechnol.* **2005**, *23* (1), 83−87.
(42) Guo, F.; Li, P.; French, J. B.; Mao, Z.; Zhao, H.; Li, S.; Nama, N.; Fick, J. R.; Benkovic, S. J.; Huang, T. J. *Proc. Natl. Acad. Sci. U. S. A.* **2015**, *112*, 43−48.
(43) Li, P.; Mao, Z.; Peng, Z.; Zhou, L.; Chen, Y.; Huang, P.; Truica, C. I.; Drabickd, J. J.; El-Deiry, W. S.; Dao, M.; Suresh, S.; Huang, T. J. *Proc. Natl. Acad. Sci. U. S. A.* **2015**, *112*, 4970−4975.
(44) Li, S.; Guo, F.; Chen, Y.; Ding, X.; Li, P.; Wang, L.; Cameron, C. E.; Huang, T. J. *Anal. Chem.* **2014**, *86* (19), 9853−9859.
(45) Johansson, L.; Nikolajeff, F.; Johansson, S.; Thorslund, S. *Anal. Chem.* **2009**, *81* (13), 5188−5196.
(46) Schmid, L.; Weitz, D. A.; Franke, T. *Lab Chip* **2014**, *14* (19), 3710−3718.
(47) Shi, J.; Mao, X.; Ahmed, D.; Colletti, A.; Huang, T. J. *Lab Chip* **2008**, *8* (2), 221−223.
(48) Shi, J.; Huang, H.; Stratton, Z.; Huang, Y.; Huang, T. J. *Lab Chip* **2009**, *9* (23), 3354−3359.
(49) Shi, J.; Yazdi, S.; Lin, S.-C. S.; Ding, X.; Chiang, I.-K.; Sharp, K.; Huang, T. J. *Lab Chip* **2011**, *11* (14), 2319−2324.
(50) Lin, S.-C. S.; Mao, X.; Huang, T. J. *Lab Chip* **2012**, *12*, 2766.
(51) Ding, X.; Lin, S.-C. S.; Kiraly, B.; Yue, H.; Li, S.; Chiang, I.-K.; Shi, J.; Benkovic, S. J.; Huang, T. J. *Proc. Natl. Acad. Sci. U. S. A.* **2012**, *109*, 11105−11109.
(52) Ding, X.; Peng, Z.; Lin, S.-C. S.; Geri, M.; Li, S.; Li, P.; Chen, Y.; Dao, M.; Suresh, S.; Huang, T. J. *Proc. Natl. Acad. Sci. U. S. A.* **2014**, *111* (36), 12992−12997.
(53) Mao, X.; Nawaz, A. A.; Lin, S.-C. S.; Lapsley, M. I.; Zhao, Y.; McCoy, J. P.; El-Deiry, W. S.; Huang, T. J. *Biomicrofluidics* **2012**, *6* (2), 024113.
(54) Nawaz, A. A.; Zhang, X.; Mao, X.; Rufo, J.; Lin, S.-C. S.; Guo, F.; Zhao, Y.; Lapsley, M.; Li, P.; McCoy, J. P.; Levine, S. J.; Huang, T. J. *Lab Chip* **2014**, *14* (2), 415−423.
(55) Nawaz, A. A.; Nissly, R. H.; Li, P.; Chen, Y.; Guo, F.; Li, S.; Shariff, Y. M.; Qureshi, A. N.; Wang, L.; Huang, T. J. *Ann. Biomed. Eng.* **2014**, *42* (11), 2303−2313.
(56) Mao, X.; Lin, S.-C. S.; Dong, C.; Huang, T. J. *Lab Chip* **2009**, *9* (11), 1583−1589.
(57) Mao, X.; Waldeisen, J. R.; Huang, T. J. *Lab Chip* **2007**, *7* (10), 1260−1262.
(58) Xia, Y.; Whitesides, G. M. *Annu. Rev. Mater. Sci.* **1998**, *28* (1), 153−184.
(59) Zhao, C.; Liu, Y.; Zhao, Y.; Fang, N.; Huang, T. J. *Nat. Commun.* **2013**, *4*, 2305.
(60) Zhao, Y.; Stratton, Z. S.; Guo, F.; Lapsley, M. I.; Chan, C. Y.; Lin, S.-C. S.; Huang, T. J. *Lab Chip* **2013**, *13* (1), 17−24.
(61) Zhao, Y.; Lin, S.-C. S.; Nawaz, A. A.; Kiraly, B.; Hao, Q.; Liu, Y.; Huang, T. J. *Opt. Express* **2010**, *18* (22), 23458−23465.
(62) Jakobsson, O.; Grenvall, C.; Nordin, M.; Evander, M.; Laurell, T. *Lab Chip* **2014**, *14* (11), 1943−1950.
(63) Ding, X.; Li, P.; Lin, S. S.; Stratton, Z. S.; Nama, N.; Guo, F.; Slotcavage, D.; Mao, X.; Shi, J.; Costanzo, F.; Huang, T. J. *Lab Chip* **2013**, *13*, 3626−3649.

DOI: 10.1021/acs.analchem.5b02398
Anal. Chem. 2015, 87, 12051−12058